A PHYSICALLY-CONSTRAINED SOURCE MODEL FOR FDTD ACOUSTIC SIMULATION

Jonathan Sheaffer,

Acoustics Research Centre
School of Computing, Science and Engineering
University of Salford
Salford, UK
j.sheaffer@edu.salford.ac.uk

Maarten Van Walstijn,

Sonic Arts Research Centre
School of Electronics, Electrical Engineering,
and Computer Science. Queen's University Belfast
Belfast, UK
m.vanwalstijn@qub.ac.uk

Bruno Fazenda,

Acoustics Research Centre
School of Computing, Science and Engineering
University of Salford
Salford, UK
b.m.fazenda@salford.ac.uk

ABSTRACT

The Finite Difference Time Domain (FDTD) method is becoming increasingly popular for room acoustics simulation. Yet, the literature on grid excitation methods is relatively sparse, and source functions are traditionally implemented in a *hard* or *additive* form using arbitrarily-shaped functions which do not necessarily obey the physical laws of sound generation. In this paper we formulate a source function based on a small pulsating sphere model. A physically plausible method to inject a source signal into the grid is derived from first principles, resulting in a source with a near-flat spectrum that does not scatter incoming waves. In the final discrete-time formulation, the source signal is the result of passing a Gaussian pulse through a digital filter simulating the dynamics of the pulsating sphere, hence facilitating a physically correct means to design source functions that generate a prescribed sound field.

1. INTRODUCTION

The FDTD method has recently become more popular for room acoustics simulation, very much owing to the increased processing power and memory resources of more commonly available computing hardware. This is evident in newly emerged numerical schemes [1, 2] and optimised parallel implementations [3], which provide means for more accurate and efficient modelling. In room-acoustics FDTD, one wishes to correctly excite a 3D grid for simulation of longitudinal acoustic wave propagation, which is a different challenge than excitation of other grids, for example for simulating transversely vibrating mechanical systems [4].

Traditionally, excitation functions are either imposed or superimposed onto the source occupying node. The former method is often referred to as a *hard source* injection where the pressure at the source position is directly set by the excitation function and the update equations for the acoustic medium are bypassed. The latter approach, often referred to as a *soft source*, describes a method in which the excitation function is added to the existing pressure at the source position, which has already been evaluated by the medium update equations.

Hard sources are common, most likely due to their simplicity and ease of implementation. However, the imposition of pressure directly on the grid is artificial and bears some complications. It suggests that acoustic pressure appears with no underlying physical cause, and as such, does not obey the laws of fluid dynamics. As the hard-source node scatters incoming waves, it can be loosely thought of as a sound radiating boundary node whose size corresponds to the spatial sample period. This characterisation, however, is also not precise, as such elements should adhere to boundary conditions which are not evident in the hard source formulation. For simulation of enclosed spaces, scattering caused by the hard-source node is artificial and detrimental to the result. Even when boundary reflections do not occur some artefacts may arise. Since the hard source is directly imposed on the grid, the transient change in sound pressure at the source node takes the form of the source function, which is a desired feature, as one can directly employ excitation signals that generate a prescribed pressure. However, as the equations of mass and momentum are not satisfied at the source node, the inability of air particles to effectively perform rarefaction may cause unwanted low-frequency artefacts when certain excitation signals are used [5]. Thus, we postulate that the hard source paradigm is fundamentally flawed in the sense that it does not adhere to any physical laws governing the medium or the boundaries.

The source-scattering and low-frequency problems can be overcome by employing *Soft Sources*. In such case, the excitation function is superimposed on the pressure at the source node, which causes it to be modified by the grid's impulse response [6]. Furthermore, in Yee-based schemes [7] the source function is differentiated by the staggered update equation, causing a steep roll-off at low frequencies. For schemes based on the wave equation, Karjalainen and Erkut [8] have shown that additive sources should be equivalently filtered with $H(z) = \left(1 - z^{-2}\right)$, which generates the same effect.

Schneider et al. [6] have addressed these issues by making use of *Transparent Sources* which radiate sound fields similar to hard sources but without scattering incoming waves. However, this ap-

proach requires that the grid's impulse response is measured prior to the simulation stage and compensated for during simulation. Therefore, it is more computationally expensive and less intuitive to implement. Furthermore, it has been shown that transparent sources also suffer from the same low frequency artefacts as hard sources [5].

Another concern which has not been thoroughly explored in context of multidimensional schemes, is the relation of the source magnitude to the numerical properties of the grid. When the amplitude of the excitation function is arbitrarily chosen, the magnitude of the resulting pressure field varies with sample rate. Due to the Courant criterion, the temporal sample-rate controls the physical volume of each grid cell, which must be taken into account when scaling the source signal.

In this paper we address all of these issues by introducing an integrated source excitation approach which adheres to both physical and numerical constraints, and is derived entirely from first principles. The source function is based on a theoretical point-monopole governed by a force-driven mass-damper-spring system. This mechanism conceptually resembles the output of an electro-mechanical transducer with an omnidirectional sound radiation pattern. We then show how a source can be embedded in an FDTD grid by discretising the appropriate fluid-dynamic governing equations. This results in an *additive* source injection method which is correctly scaled with FDTD parameters and is in agreement with analytic solutions to the wave equation. The entire system is represented as a set of DSP operations, which can be used to generate a prescribed pressure source function of near-flat spectrum within a controlled bandwidth.

Section 2 discusses the governing equations in the mechanical and acoustical domains. Section 3 provides a numerical formulation of the method, for both synthesising a source signal and injecting it into an FDTD grid. Results for some typical applications are shown in Section 4, followed by a discussion and conclusions.

2. GOVERNING EQUATIONS

2.1. Sound Source

We consider a pulsating sphere of (small) radius a_0 whose surface velocity $u(t)$, in vacuum, is governed by

$$M\frac{\partial u(t)}{\partial t} = -Ru(t) - K\int u(t)dt + F(t) \tag{1}$$

where M, R, and K are respectively, the mass, damping and elasticity constants characterising the mechanical system, and $F(t)$ is the force driving the sphere pulsation. With air surrounding the sphere, the mechanical impedance of the system is

$$Z(\omega) = Z_{\mathrm{v}}(\omega) + Z_{\mathrm{a}}(\omega) \tag{2}$$

where $Z_{\mathrm{v}}(\omega) = Mj\omega + R + K/(j\omega)$ is the impedance of the system in vacuum and $Z_{\mathrm{a}}(\omega) = \rho_0 A a_0 \left(j\omega - (a_0/c)\omega^2\right)$ is the mechanical impedance of the surrounding air [9, p. 315]. However, the latter term may be omitted since a_0 is very small, meaning that $|Z_{\mathrm{v}}(\omega)| >> |Z_{\mathrm{a}}(\omega)|$ in all practical cases. Hence the system may be characterised by the transfer function

$$H(s) = \frac{1}{Ms + R + K/s} \tag{3}$$

which has the dimension of mechanical admittance. In the time domain, the impulse response of the system is given by

$$h(t) = \frac{1}{Me^{\alpha t}}\left[\cos(\omega_r t) - \frac{\alpha}{\omega_r}\sin(\omega_r t)\right] \tag{4}$$

where $\alpha = \frac{R}{2M}$ is the damping factor, $\omega_0 = \sqrt{\frac{K}{M}}$ is the system's undamped resonant frequency and $\omega_r = \sqrt{\omega_0^2 - \alpha^2}$. At the source, the sphere's surface velocity equals the particle velocity of air, which can be mathematically expressed as convolution between the driving force and the system's impulse response, $u(t) = F(t) * h(t)$. The pulsation of the sphere causes fluid to be pushed into and extracted from the region bordering the source sphere surface, which is characterised by a *volume velocity*,

$$\hat{q}(t) = u(t)A_s \tag{5}$$

having the dimensions of volume per unit time ($m^3 s^{-1}$), where $A_s = 4\pi a_0^2$ is the surface area of the sphere.

2.2. Sound Generation and Propagation

The conceptual point-monopole described in section 2.1 generates a volume velocity $\hat{q}(t)$ at the source position. We shall now relate this quantity to the inhomogeneous wave equation,

$$\frac{1}{c^2}\frac{\partial^2 p(\mathbf{x},t)}{\partial t^2} - \nabla^2 p(\mathbf{x},t) = \psi(\mathbf{x},t) \tag{6}$$

which is used to describe the sound field at $\mathbf{x} = (x,y,z) \in \mathbb{R}^3$. In order to enable direct comparison with other studies, we define $\psi(\mathbf{x},t)$ as a general source driving function which can take on any form or shape. In this section we aim to derive an appropriate ψ which will obey the physical laws of fluid emergence, by first considering the conservation laws of mass and momentum. In their Eulerian form, the continuity and momentum equations with sources are given by [9, p. 241]

$$\frac{\partial \rho(\mathbf{x},t)}{\partial t} + \rho_0 \nabla \cdot \mathbf{u}(\mathbf{x},t) = q(\mathbf{x},t) \tag{7}$$

$$\rho_0 \frac{\partial \mathbf{u}(\mathbf{x},t)}{\partial t} + \nabla p(\mathbf{x},t) = \widetilde{\mathbf{F}}(\mathbf{x},t) \tag{8}$$

Where ρ_0 is the ambient density of air, $\rho(\mathbf{x},t)$ is the transient change of density, and $\mathbf{u}(\mathbf{x},t)$ and $p(\mathbf{x},t)$ are the particle velocity and pressure respectively. Here, the function $q(\mathbf{x},t)$ denotes the rate of fluid emergence in the system in the dimensions of density per unit time (kg m^{-3} s^{-1}), and the function $\widetilde{\mathbf{F}}(\mathbf{x},t)$ is the *acoustic* force exerted upon the source volume (not to be confused with the mechanical force driving the sphere pulsation). In the problem discussed in this paper, the sound source is considered to be an acoustic transducer converting mechanical forces into volume velocity. Therefore, it is reasonable to treat $q(\mathbf{x},t)$ as the primary source generating function, and the force term in equation (8) is neglected. Considering now a source positioned at a single node of an FDTD grid, in which each cell occupies a volume equal to X^3, we can relate the volume velocity of the source $\hat{q}(t)$ to the source density term $q(\mathbf{x},t)$ as follows

$$q(\mathbf{x},t) = \frac{\rho_0}{X^3}\hat{q}(t)\delta(\mathbf{x} - \mathbf{x}') \tag{9}$$

where $\mathbf{x}' = (x',y',z') \in \mathbb{R}^3$ denotes the source position. As will be demonstrated in section 4.2, using the relationship in equation

(9) results in correct magnitude scaling of the source signal. To express equation (7) as a function of acoustic pressure, it is assumed that $\|\mathbf{u}\| \ll c$ and the equation of state $p(\mathbf{x},t) = c^2\rho(\mathbf{x},t)$ can be used to convert density to pressure, yielding

$$\frac{\partial p(\mathbf{x},t)}{\partial t} = -\rho_0 c^2 \nabla \cdot \mathbf{u}(\mathbf{x},t) + c^2 q(\mathbf{x},t) \tag{10}$$

By combining equations (8) and (10), the particle velocity vector is eradicated and the wave equation (6) is derived (note that here equation (8) is used without the acoustic force term). It follows from this derivation that the source term becomes

$$\psi(\mathbf{x},t) = \frac{\partial q(\mathbf{x},t)}{\partial t} = \frac{\rho_0}{X^3}\frac{d}{dt}\hat{q}(t)\delta(\mathbf{x}-\mathbf{x}') \tag{11}$$

Physically, the quantity $\psi(\mathbf{x},t)$ has the dimensions of density per unit time squared (kg m^{-3} s^{-2}), and can be thought of as fluid emergence due to volume acceleration of the source.

In a spherically-symmetrical system, an analytic solution for (6) in free field is possible. In such case, the spherical Laplace operator in (6) becomes angle-independent, and with a point-source approximation, the sound pressure at the distance $r = \|\mathbf{x}-\mathbf{x}'\|$ is given by [9, p. 310]

$$p(r,t) = \frac{\rho_0}{4\pi r}\frac{d}{dt}\hat{q}\left(t - \frac{r}{c}\right) \tag{12}$$

For $\hat{q}(t) = \delta(t-t')$, equation (12) is the transient free-field Green's function solution to the wave equation.

3. NUMERICAL FORMULATION

In this section we present the proposed source formulation in the numerical domain. Here it is applied to a family of schemes for the wave equation which have been shown to be efficient in simulating room acoustics [1]. A similar formulation is possible for other schemes.

3.1. Compact Explicit Schemes

The wave equation (6) can be modelled using centred finite difference (FD) operators as

$$\left(\delta_t^2 - \lambda^2\delta_{\mathbf{x}}^2\right) p_{\mathbf{i}}^n = \underbrace{c^2T^2\psi_{\mathbf{i}}^n}_{\text{Source Term}} \tag{13}$$

where X is the spatial sample period, T is the temporal sample period, $\lambda = cT/X$ is the Courant number, and the pressure field is discretised such that

$$p\big|_{\mathbf{i}}^n = p(x,y,z,t)\big|_{x=lX,y=mX,z=iX,t=nT} \tag{14}$$

The discrete FD operators are given by

$$\delta_t^2 p_{\mathbf{i}}^n \equiv p\big|_{\mathbf{i}}^{n+1} - 2p\big|_{\mathbf{i}}^n + p\big|_{\mathbf{i}}^{n-1} \tag{15}$$

$$\delta_x^2 p_{\mathbf{i}}^n \equiv p\big|_{l+1,m,i}^n - 2p\big|_{l,m,i}^n + p\big|_{l-1,m,i}^n \tag{16}$$

$$\delta_y^2 p_{\mathbf{i}}^n \equiv p\big|_{l,m+1,i}^n - 2p\big|_{l,m,i}^n + p\big|_{l,m-1,i}^n \tag{17}$$

$$\delta_z^2 p_{\mathbf{i}}^n \equiv p\big|_{l,m,i+1}^n - 2p\big|_{l,m,i}^n + p\big|_{l,m,i-1}^n \tag{18}$$

where the spatial index vector $\mathbf{i}$ and operator $\delta_{\mathbf{x}}^2$ are given by

$$\mathbf{i} = [l,m,i] \tag{19}$$

$$\delta_{\mathbf{x}}^2 = \delta_x^2 + \delta_y^2 + \delta_z^2 + a\left(\delta_x^2\delta_y^2 + \delta_x^2\delta_z^2 + \delta_y^2\delta_z^2\right) + b\delta_x^2\delta_y^2\delta_z^2 \tag{20}$$

The free parameters a and b are chosen according to the desired numerical properties, which for $a = 0,\ b = 0$ results in the well known *standard rectilinear* grid. For the source node, the driving function ψ is given in the discrete domain by

$$\psi_{\mathbf{i}'}^n = \frac{\rho_0}{X^3 2T}\left(\hat{q}\big|^{n+1} - \hat{q}\big|^{n-1}\right) \tag{21}$$

and accordingly, equation (13) can be expressed in additive form as follows

$$p\big|_{l',m',i'}^{n+1} = \left\{p\big|_{l',m',i'}^{n+1}\right\} + \frac{\rho_0 c\lambda}{2X^2}\left(\hat{q}\big|^{n+1} - \hat{q}\big|^{n-1}\right) \tag{22}$$

where $p\big|_{l',m',i'}^{n+1}$ is the pressure at the source node and $\left\{p\big|_{l',m',i'}^{n+1}\right\}$ represents the result of updating the node with the regular air update equation (see Appendix I). The apostrophe symbols above spatial indices denote that the equation is evaluated at the source node.

3.2. Representation in the Z-Domain

In the discrete domain, equation (22) requires that the volume velocity, $\hat{q}\big|^n$ is obtained from $u\big|^n$. This function can be generated by discretising the convolution of a specified driving force $F(t)$ with the impulse response of the system (4). However, we may represent the system directly in the z-domain, avoiding the need to explicitly perform convolution in the time-domain. Here we opt to apply the bilinear transform in order to obtain the z-domain transfer function of the system. This choice is mainly because, unlike other discretisation methods, the bilinear transform does not place any stability limits on the values of M, R and K, thus allowing them to be freely chosen. The bilinear transform of equation (3) is

$$H(s)\big|_{s=\beta\frac{1-z^{-1}}{1+z^{-1}}} = \tag{23}$$

$$\frac{\beta\left(1-z^{-2}\right)}{\left(M\beta^2+R\beta+K\right) + \left(2K-2M\beta^2\right)z^{-1} + \left(M\beta^2-R\beta+K\right)z^{-2}}$$

where β is the bilinear operator, which for a pre-warped ω_0 is given by

$$\beta = \frac{\omega_0}{\tan(\omega_0 T/2)} \tag{24}$$

Normalising (23) we can express the system in a form of a digital filter

$$H(z) = \frac{b_0 + b_2 z^{-2}}{1 + a_1 z^{-1} + a_2 z^{-2}} \tag{25}$$

With the coefficients given by

$$b_0 = \frac{\beta}{M\beta^2 + R\beta + K} \tag{26}$$

$$b_2 = -\frac{\beta}{M\beta^2 + R\beta + K} \tag{27}$$

$$a_1 = \frac{2\left(K - M\beta^2\right)}{M\beta^2 + R\beta + K} \tag{28}$$

$$a_2 = 1 - \frac{2R\beta}{M\beta^2 + R\beta + K} \tag{29}$$

In the discrete domain, a driving force $F\big|^n$ can be simply filtered with (25) to obtain the surface velocity of the source. Then, it follows from equations (5) and (9) that the filtered result is multiplied

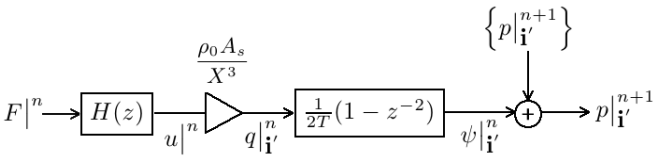

Figure 1: *DSP block diagram of source generation and injection.* $F\big|^n$ *denotes driving force,* $H(z)$ *is the transfer function of the point-monopole model,* $u\big|^n$ *denotes surface velocity,* $q\big|^n$ *denotes the rate of fluid emergence in the system,* $\psi\big|^n$ *denotes the source function,* $\{p|^{n+1}_{i'}\}$ *is the regular update equation for air, and* $p|^{n+1}_{i'}$ *is the resulting sound pressure at the source node.*

by $\rho_0 A_s/X^3$ to directly obtain $q\big|^n_{\mathbf{i}'}$. The complete signal processing required for generating and injecting the source into the grid is graphically shown in figure 1. Note that the processing shown in figure 1 outputs a signal which is delayed by one-sample in comparison to the result of equation (22). In this paper we refer to the entire model presented here as a *Physically-Constrained Source*, abbreviated *PCS* hereafter.

4. RESULTS

4.1. Prescribed Pressure Source

In room acoustics simulation, it is desirable to design a source function that generates a prescribed sound field. In this section we show how the *Physically-Constrained Source* (PCS) can be used to accomplish this task. The goal is to design an excitation signal that propagates omni-directionally and has a flat frequency response within a defined frequency range. It is not possible (nor physically practical) to implement a source mechanism with infinite bandwidth. Nevertheless, some properties of the system can be exploited to effectively band-limit the excitation signal whilst still maintaining a near-flat frequency response within its passband.

The low-frequency behaviour of the source is characterised by the system resonance ω_0 and quality factor Q. The former controls the low cut-off frequency whilst the latter defines the steepness of the transition between the rolled-off frequencies and the passband. In an optimal transducer design process, the designer would specify the desired values for these parameters and the remaining electro-mechanical quantities would be engineered accordingly. In the model presented herein, it is assumed that the source has some mass, M, and the remaining damping and stiffness coefficients are then calculated from $R = \frac{\omega_0 M}{Q}$ and $K = M\omega_0^2$, respectively. Since all FDTD schemes exhibit numerical dispersion, at least to some extent, it is also desired to specify a high cut-off frequency. This can be achieved by employing a driving function with a Gaussian force distribution, given by

$$F(t) = Ae^{-\frac{(t-t')^2}{2\sigma^2}} \tag{30}$$

where A is the amplitude of the pulse, t' is the initial time delay, σ is the variance. Figure 2 shows the modelled behaviour of such a system in the time-domain, in terms of the exerted force and resulting surface displacement and velocity. The surface velocity, $u(t)$ and corresponding volume velocity, $\hat{q}(t)$ were obtained by filtering the driving force function $F(t)$ using equation (25).

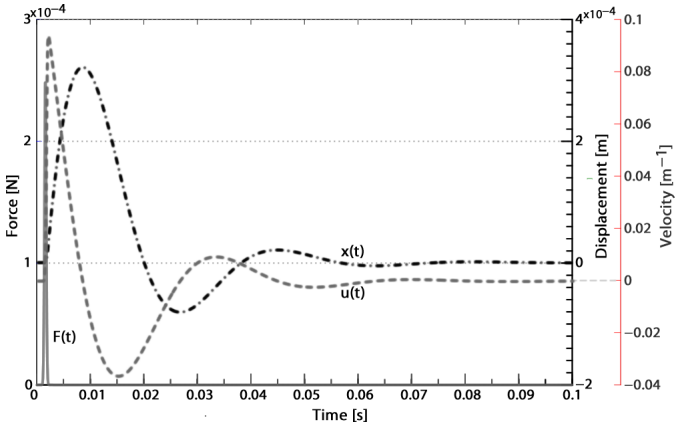

Figure 2: *Surface velocity u(t), and surface displacement* $x(t) = \int u(t)dt$ *for a pulsating sphere driven by a Gaussian force,* $F(t)$*. Note that the y-axes are slightly displaced for visual clarity.*

In this example we have considered a source whose surface mass is $M = 25$g, and area $A_s = 6X^2$ corresponds to the surface area of a single FDTD grid cell, which is numerically equivalent to a pulsating sphere of radius $a_0 = \sqrt{1.5/\pi}X$. The band-limiting parameters are set to $f_0 = 30$Hz, $Q = 1.25$ and $\sigma = 9.25 \cdot 10^{-5}$; and the driving function has an amplitude of $A = 250\mu$N. The source was placed at the centre of an FDTD grid solved using the *Interpolated Wideband* (IWB) scheme, with the free parameters set to $a = 1/4$, $b = 1/16$ and $X = 28.62$mm. The transient sound pressure, obtained at the receiving position 0.5m away from the source in the axial direction, is shown in figure 3. For comparison purposes, the sound pressure at the receiving position was also calculated in closed form using equation (12), and is shown as reference (solid line) in figure 3.

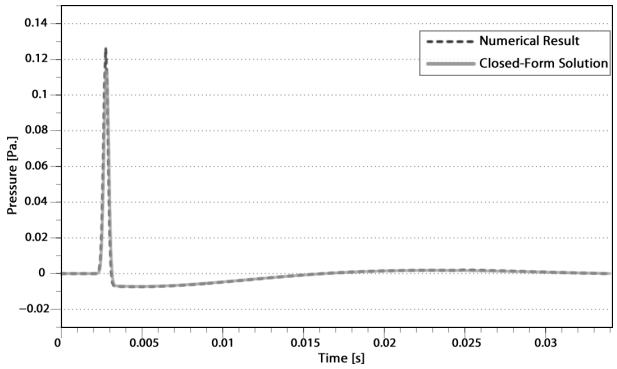

Figure 3: *Sound pressure response at the receiving position. Numerical results (dashed line) are compared to the closed-form solution* (12) *to the wave equation (solid line).*

To exemplify high-frequency effects, we define a variable η denoting a normalised high cut-off frequency, which is related to the Gaussian variance by $\sigma = 1/(\eta f_s)$. Figure 4 shows the frequency response at the receiving position for three cases of η. It can be seen that for low values of η, corresponding to highly oversampled solutions, numerical results almost perfectly converge with the closed form solution. As one would expect, at high frequen-

cies the discrepancy increases, which is particularly visible for the largest value of η. This is attributed to the fact that whilst the analytic solution assumes spherical symmetry, the dispersive properties of the FDTD method cause anisotropy that grows stronger as frequency is increased. The choice of η is therefore a compromise between bandwidth and the amount of dispersion introduced by high frequencies.

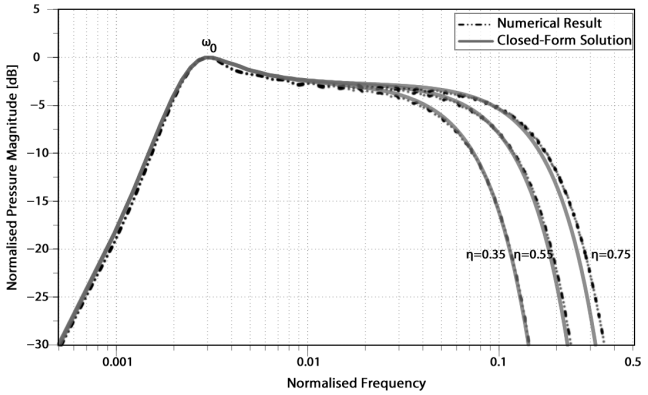

Figure 4: *Frequency response of the sound pressure at the receiving position. Numerical results (dashed lines) are compared to closed-form solutions* (12) *to the wave equation (solid lines).*

The effects of Q on the low frequency behaviour of the system are shown in figure 5. As expected, the higher Q is, the more pronounced is the low-frequency resonance of the system. It can be

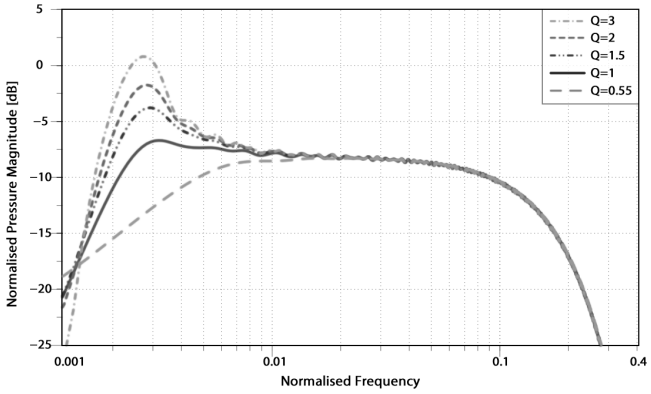

Figure 5: *Frequency response at the receiving position with* $Q = 0.55$ *(heavy dashed),* $Q = 1$ *(solid),* $Q = 1.5$ *(triple dashed),* $Q = 2$ *(dashed) and* $Q = 3$ *(double dashed). The high cut-off is set* $\eta = 0.75$ *for all curves.*

seen that the flatness of the response at low frequencies is strongly affected by the choice of Q, in a similar fashion to a real-world transducer. At $Q = 0.55$, when the system is nearly critically damped, the magnitude response rolls off as a near straight line. Making Q higher allows extending the low frequency bandwidth at the expense of a more pronounced resonance and a more abrupt transition. This is the type of compromise that a loudspeaker designer faces when choosing a driver and enclosure. In such cases, the total Q of the electro-mechanical system typically ranges between 0.5 and 2.0 [10].

4.2. Numerical Consistency

An important feature of the PCS model is that it yields consistent results across different sample rates. Since the source function is correctly scaled with FDTD grid parameters (see equation 9), then for a given volume velocity the resulting pressure is independent of sample rate. Clearly, if the source area A_s is chosen such that it varies with the spatial sample period, then so will the corresponding volume velocity and the resulting pressure at the source position. Thus, if one wishes to preserve numerical consistency, then A_s should be held constant even if the sample rate is changed.

To test this, two simulations were carried out at grid resolutions of $X = 19$mm and $X = 10.7$mm. Since the total source energy depends on the variance of the Gaussian driving force which normally depends on f_s as well as η, here a constant σ was maintained in order to ensure that an identical amount of energy was injected into the grid at both resolutions. Simulations were repeated for three types of sources. First, we examine the typical *hard source* method in which the driving function, $\psi(t)$, is directly imposed on the source grid node, i.e

$$p|^{n+1}_{l',m',i'} = \psi|^{n+1} \tag{31}$$

where in this case ψ is simply considered to be a Gaussian function. Next, we test a *soft source* derived from a 1D waveguide analysis as presented in [8], with $\hat{q}(t)$ being differentiated, scaled and superimposed on the source node, such that:

$$p|^{n+1}_{l',m',i'} = \left\{p|^{n+1}_{l',m',i'}\right\} + \psi|^{n+1} \tag{32}$$

where $\psi|^{n+1} = \frac{\rho_0 c}{2X}\left(\hat{q}|^{n+1} - \hat{q}|^{n-1}\right)$, and $\hat{q}$ is considered to be a volume velocity with a Gaussian distribution to which the physical model presented herein has *not* been applied. Lastly, we consider the *physically-constrained source* model with A_s kept constant across the two different grid resolutions.

It can be seen from figure 6 that whilst the hard and soft sources exhibit different pressure magnitudes at the receiving position, the amplitude of the physically-constrained source remains identical at different grid resolutions. It should be noted, however, that for a one-dimensional waveguide, one would expect a similar behaviour from a soft source given that it has been appropriately scaled as shown in [8].

4.3. Frequency Response

The frequency response curves of the three different source models described in 4.2 are shown in figure 7. Here, the pulsating sphere system was designed with its natural resonance at the normalised frequency $f_0T = 0.002$, and $Q = 1$. It can be seen that the frequency response of the PCS is nearly as flat as the hard source. The soft source exhibits the frequency response of a differentiated Gaussian, as it lacks the mechanical filter included in the PCS formulation.

4.4. DC Effects

When an excitation signal is injected in an additive form, it must not contain a DC component otherwise a growing solution will occur. This growth is strongly linked to source-boundary interaction, and unlike more typical growth problems, is unrelated to numerical stability. For simplicity, consider a source placed in front of a reflecting surface on the x-plane. For a plane wave source

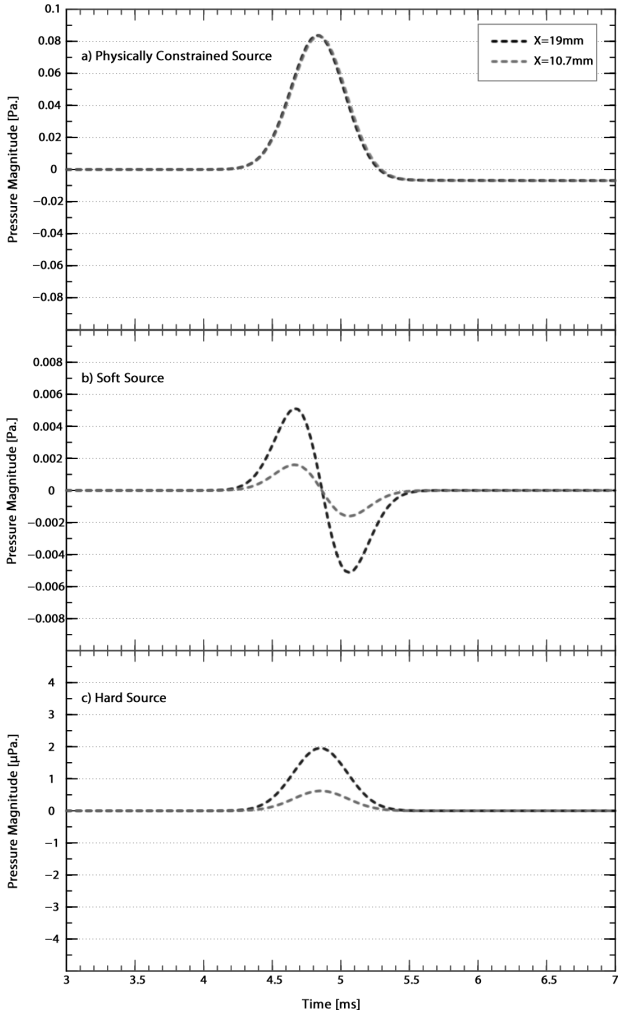

Figure 6: *Impulse responses generated at grid resolutions of $X = 19$mm (dark curves) and $X = 10.7$mm (light curves), for a) Physically constrained source, b) Soft Source and c) Hard Source. Simulations performed with $f_0 = 30$Hz, $M = 25$g and $Q = 1.25$. The force driving function is a Gaussian pulse which is identical in shape to panel (c). A more detailed evaluation of the driving function is shown in Figure 2.*

of arbitrary amplitude A, interacting with a surface having a reflection coefficient $\hat{r}$, the total sound pressure along the plane is $p(x,t) = Ae^{j(\omega t - kx)} + \hat{r}Ae^{j(\omega t + kx)}$. As such, the sound pressure at DC is uniformly $p = A(1+\hat{r})$ along the plane. Since source injection is additive, then for any $\hat{r} > 0$ a pre-existing DC component would constructively superimpose on itself at the source node, resulting in an incremental offset.

To exemplify this, consider an additive source injection as shown in equation (32), driven directly by a Gaussian excitation function, such that

$$\psi(t) = Ae^{-\frac{(t-t')^2}{2\sigma^2}} \tag{33}$$

Being a unipolar function, the Gaussian source exhibits a strong DC component, thus we expect solution growth. Unlike the soft

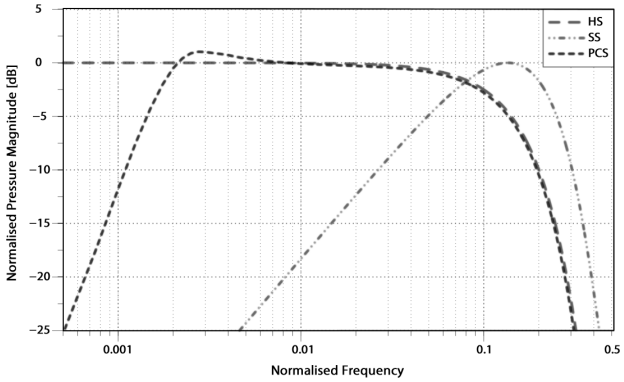

Figure 7: *Frequency response of three types of sources: Hard Source (HS, heavy dashed), Soft Source after Karjalainen and Erkut [8] (SS, triple dashed-dotted) and Physically-Constrained Source as presented in this paper (PCS, regular dashed). All sources were generated with $\eta = 0.75$, and the PCS was designed with a normalised resonance at $f_0 T = 0.002$ and $Q = 1$.*

source described in section 4.2, this function does not get differentiated prior to being injected in additive form, and as such, will be further referred to as an *Arbitrary Soft Source*. As reference, consider the same excitation function, however being filtered and injected according to the PCS principles, which is summarised in Figure 1. As will be further discussed, the PCS model acts as a natural DC-blocking filter, therefore no solution growth is expected. The result of this comparison is shown in Figure 8.

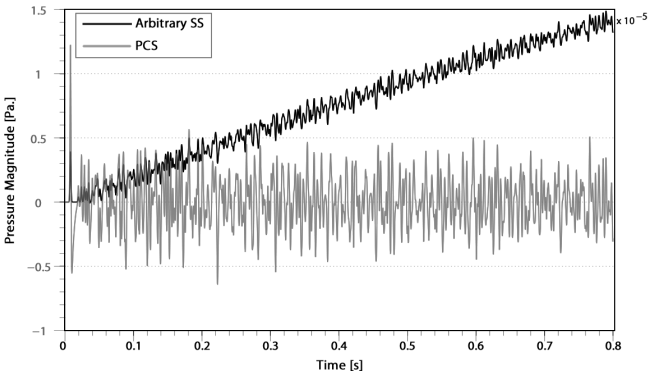

Figure 8: *Sound pressure response at the receiving position, due to an arbitrary soft source (SS - dark solid line) plotted against a physically constrained source (PCS - light solid line). Note that the magnitude scale of the soft source is different. Both simulations where executed with uniform boundary conditions corresponding to $\hat{r} = 0.997$.*

Such behaviour is also sensible from a physical perspective, as a DC component in $\psi(t)$ indicates that $q(t)$ is not of finite length, meaning that the source endlessly generates volume velocity. Following equation (11), the rate of fluid emergence due to the arbitrary soft source is obtained by taking the integral of equation (33) which yields

$$q(t) = \int \psi(t)dt = \sqrt{\frac{\pi}{2}} A\sigma \mathrm{ERF}\left(\frac{t-t'}{\sqrt{2}\sigma}\right) \tag{34}$$

where ERF$(\cdot)$ is the Gauss error function. Figure 9 shows the comparison of an additive function $\psi(t)$ plotted against its corresponding rate of fluid emergence $q(t)$, for an arbitrary soft source (after equations (33) and (34)) and a physically constrained source. Similar effects have been observed in the field of computational electrodynamics [11]

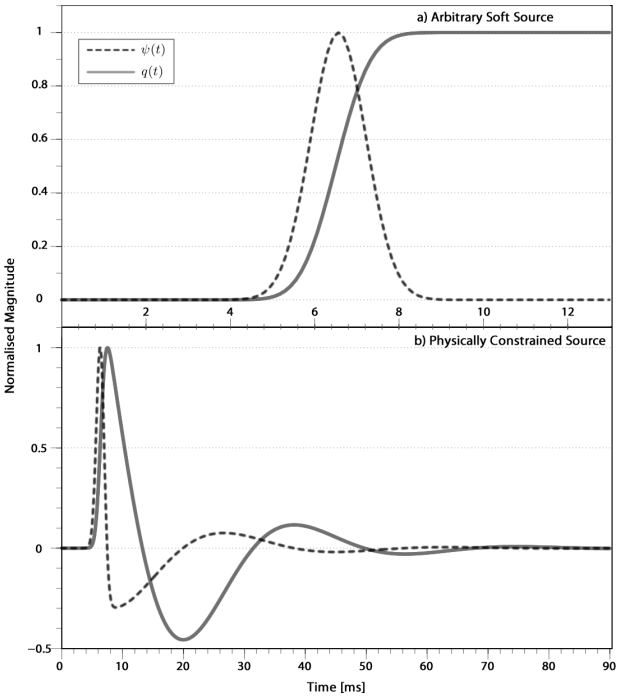

Figure 9: *Comparison of $\psi(t)$ and $q(t)$ for two source models, a) arbitrary soft source directly driven by a Gaussian function; and b) physically-constrained source driven by a Gaussian force. Results have been normalised for visual clarity.*

For the PCS, both $q(t)$ and $\psi(t)$ start at zero and decay to zero, indicating a finite source. However, this is not the case for the arbitrary soft source. The fact that $\psi(t)$ seems time-limited can be misleading, as it only physically means that the source generating mechanism does not accelerate before or after the excitation period. This, of course, does not mean that the source is not active. In fact, it can be seen that when $\psi(t)$ decays, $q(t)$ rises and stays at a constant value through the remaining simulation period. This indicates that even when $\psi(t)$ is time limited, the source mechanism may still generate volume velocity. As one would expect, $q(t)$ remains at a constant positive value which is equivalent to generation of DC.

5. DISCUSSION

The PCS model described in this paper provides means to design sources of prescribed pressure. In a free field, results show very good matching with the closed-form solution to the wave equation, which underlines the physical basis of the approach. Discrepancies are mostly attributed to the numerical artefacts of the system, which include spatial quantisation and dispersion. Both of these can be greatly reduced by means of oversampling, choosing an appropriate numerical scheme, and/or spatial interpolation. To demonstrate the benefits of the PCS model, we have used a Gaussian pulse as a driving force. The source signal is truncated at points chosen such that the resulting discontinuity errors largely fall below the numerical errors due to the finite difference approximations. Consequently, such an excitation function is a suitable candidate for the requirements of an FDTD source, as it is both band-limited *and* sufficiently time-limited. The model is also applicable to other excitation signals.

The importance of scaling and differentiating additive sources has been clearly identified in this work. Correct magnitude scaling of the excitation signal is essential for obtaining consistent results when numerical parameters are altered. More importantly, the magnitude scaling of the PCS model yields results that converge well with the analytic solution, which is not the case for other sources. The model inherently handles differentiation of the source function, which eliminates the DC component from the source term, thus avoiding any undesirable signal growth. Following equation (11), the source function in the frequency domain is $\Psi(\omega) = j\omega Q(\omega)$, which is null for $\omega = 0$. This requires that $q(\mathbf{x}, t)$ is differentiable in time and that $q(\mathbf{x}, \pm\infty) = 0$. The former can be satisfied by choosing a sufficiently smooth driving function. The latter criterion requires that the pulsating sphere begins at its resting position and returns to that position after the excitation period. Close observation of equation (4) shows that

$$\lim_{t\to\infty} Me^{-\alpha t} = 0 \quad , \quad \forall\alpha > 0 \tag{35}$$

therefore if $F(t)$ begins and ends at zero, and α is positive, then both $q(t)$ and $\psi(t)$ are appropriately time-limited, as has been shown to be the case in section 4.4. A suitable $F(t)$ can be obtained by employing an adequately finite function with $t' > 0$. A positive α simply means that the mechanical system must be damped. This affirms that the pulsating sphere model acts as a natural DC blocking filter.

Similar issues concerning scaling and differentiation have been briefly discussed in [8]. However, being drawn from 1D digital waveguide theory, the proposed scaling is inadequate for 3D schemes. Furthermore, an appropriate excitation signal is not explicitly defined. It has been shown that employing an arbitrary excitation signal in additive form can result in solution growth (see figure 8), or if it has been differentiated then the observed pressure signal is high-pass filtered (see figure 7). In the PCS model, the mass reactance of the sphere acts as an integrator which, in a physical manner, counters the effects of differentiation. Below its resonant frequency, the system is stiffness dominated, and as such, naturally acts as a DC-blocking filter. The result is a source having a near-flat pressure spectrum (see Figure 4) whose physical properties can be freely chosen by adjusting Q and ω_0. Thus, the PCS model adheres to physical laws but is not limited by real-world engineering constraints. Technically, it is possible to empirically design a source function which is compatible with an arbitrary soft-source injection by passing the excitation signal through a simple DC-blocker with the transfer function $H(z) = (1 - z^{-1})/(1 - az^{-1})$. For differentiated soft-sources, one may also consider using the first time integral of any function which does not have a DC component. Yet, the PCS method offers a more structured and physically-oriented approach for achieving these goals.

In comparison to a hard source, the spectrum of the PCS is not flat down to DC, however the low-frequency roll off is essential as it has been shown that a DC component is undesirable. Transparent sources radiate sound fields similar to hard sources without

scattering incoming waves, thus as far as frequency response is concerned, they offer a good alternative to the PCS method. However, the PCS method also physically relates the excitation function to grid parameters, and as such, is the only method which is numerically consistent by default. Furthermore, transparent sources are more computationally expensive, and are prone to the same low frequency artefacts as hard sources [5], which is not the case of the PCS.

6. CONCLUSION

In the numerical domain, the source model described in this paper can be thought of as a *discrete point-monopole* which is constrained by physical laws. Two systems govern the source, the first being the mechanical pulsation of a small sphere, and the second being the transduction of motion into acoustic pressure. To the authors' knowledge, this is the first time where these two systems have been integrated into a single physically-plausible model, at least in context of FDTD simulation. This approach offers various benefits over existing source models. It provides means to design and inject sources which generate a prescribed pressure field, do not scatter incoming waves, and have a near-flat frequency response without causing any low-frequency artefacts. Furthermore, the method is correctly scaled with FDTD parameters, and thus is numerically consistent across different sample rates. The two systems governing the source are uncoupled, which is a reasonable assumption as the pulsating sphere is considered to be very small. A more realistic model would consider numerical coupling of the two systems, which remains an interesting topic for future research.

7. ACKNOWLEDGMENTS

The authors would like to thank Mark Avis for insightful discussions on sound generating mechanisms, and three anonymous reviewers for their valuable comments and suggestions.

8. REFERENCES

[1] K. Kowalczyk and M. van Walstijn, "Room acoustics simulation using 3-D compact explicit FDTD schemes," *IEEE Transactions on Audio, Speech, and Language Processing*, vol. 19, no. 1, pp. 34–46, 2011.

[2] S. Bilbao, "Optimized FDTD schemes for 3D acoustic wave propagation," *IEEE Transactions on Audio, Speech, and Language Processing*, , no. 99, pp. 1–1, 2012.

[3] L. Savioja, "Real-time 3D finite-difference time-domain simulation of low-and mid-frequency room acoustics," in *13th Int. Conf on Digital Audio Effects*, 2010.

[4] F. Fontana and D. Rocchesso, "Physical modeling of membranes for percussion instruments," *Acta Acustica united with Acustica*, vol. 84, no. 3, pp. 529–542, 1998.

[5] H. Jeong and Y.W. Lam, "Source implementation to eliminate low-frequency artifacts in finite difference time domain room acoustic simulation," *Journal of the Acoustical Society of America*, vol. 131, no. 1, pp. 258, 2012.

[6] J.B. Schneider, C.L. Wagner, and S.L. Broschat, "Implementation of transparent sources embedded in acoustic finite-difference time-domain grids," *The Journal of the Acoustical Society of America*, vol. 103, pp. 136, 1998.

[7] D. Botteldooren, "Finite-difference time-domain simulation of low-frequency room acoustic problems," *The Journal of the Acoustical Society of America*, vol. 98, pp. 3302, 1995.

[8] M. Karjalainen and C. Erkut, "Digital waveguides versus finite difference structures: Equivalence and mixed modeling," *EURASIP Journal on Applied Signal Processing*, vol. 2004, pp. 978–989, 2004.

[9] P.M.C. Morse and K.U. Ingard, *Theoretical acoustics*, Princeton Univ Pr, 1986.

[10] R. H. Small, "Closed-box loudspeaker systems-part 1: Analysis," *J. Audio Eng. Soc*, vol. 20, no. 10, pp. 798–808, 1972.

[11] T. Su, W. Yu, and R. Mittra, "A new look at FDTD excitation sources," *Microwave and optical technology letters*, vol. 45, no. 3, pp. 203–207, 2005.

9. APPENDIX I: UPDATE EQUATION FOR AIR

The update equation for air, $\left\{p|^{n+1}_{l',m',i'}\right\}$, is required in order to evaluate the source node in an additive form. Readers who wish to implement the compact explicit schemes discussed in section 3.1 may use the following air update equation:

$$p|^{n+1}_{l,m,i} = d_4 p|^{n}_{l,m,i} - p|^{n-1}_{l,m,i} + d_1 \underbrace{\sum p|_a}_{axial} + d_2 \underbrace{\sum p|_{sd}}_{side\text{-}diagonal} + d_3 \underbrace{\sum p|_d}_{diagonal}$$

where $\sum p|_a$, $\sum p|_{sd}$ and $\sum p|_d$ are the sums of pressures of the neighbouring nodes at the axial, side-diagonal and diagonal directions, respectively. The coefficients d_1, d_2, d_3 and d_4 are calculated from the free parameters a and b, and are given by

$$\begin{aligned} d_1 &= \lambda^2(1 - 4a + 4b) \\ d_2 &= \lambda^2(a - 2b) \\ d_3 &= \lambda^2 b \\ d_4 &= 2 + \lambda^2 (12a - 8b - 6) \end{aligned}$$

For a complete listing of free parameters for different compact explicit schemes, readers are referred to [1].